Optics Letters

Sum rules for energy deposition eigenchannels in scattering systems

Alexey Yamilov,[1,*] Nicholas Bender,[2] and Hui Cao[3]

[1]Physics Department, Missouri University of Science & Technology, Rolla, Missouri 65409, USA
[2]School of Applied and Engineering Physics, Cornell University, Ithaca, New York 14852, USA
[3]Department of Applied Physics, Yale University, New Haven, Connecticut 06511, USA
*Corresponding author: yamilov@mst.edu

Received 4 July 2022; revised 11 August 2022; accepted 12 August 2022; posted 12 August 2022; published 16 September 2022

In a random-scattering system, the deposition matrix maps the incident wavefront onto the internal field distribution across a target volume. The corresponding eigenchannels have been used to enhance the wave energy delivered to the target. Here, we find the sum rules for the eigenvalues and eigenchannels of the deposition matrix in any system geometry: including two- and three-dimensional scattering systems, as well as narrow waveguides and wide slabs. We derive a number of constraints on the eigenchannel intensity distributions inside the system as well as the corresponding eigenvalues. Our results are general and applicable to random systems of arbitrary scattering strength as well as different types of waves including electromagnetic waves, acoustic waves, and matter waves.

https://doi.org/10.1364/OL.468697

Introduction. Wavefront shaping opened a new frontier for coherent manipulation of wave propagation in complex media [1–4]. The core idea is rooted in the determinism of coherent wave propagation in static, linear scattering media [5]. Although the incident wavefront can be optimized via an iterative optimization procedure [6], solving the eigenvalue problem of a linear operator (matrix) is a more predictive approach [7]. Recently, a number of matrices have been introduced to manipulate quantities such as transmittance, reflectance, dwell-time, spatial distribution, etc., see Refs. [4,5,8,9] for review. Control and optimization of wave energy inside a scattering medium requires an access to the internal field distribution [10]. To find the ultimate limit of energy delivery to a target buried deep inside a diffusive medium, we recently introduced a deposition matrix that relates the incident wavefront to the internal field distribution across the target [11]. The maximal eigenvalue of the matrix gives the largest possible energy enhancement, while the corresponding eigenvector gives the optimal incident wavefront. However, the properties of the deposition eigenvalues and eigenchannels remain essentially unknown.

In this work, we theoretically obtain a series of sum rules satisfied by the local intensity of the deposition eigenchannels (DEs) and their eigenvalues. In Ref. [11], DEs were decomposed into the transmission eigenchannels (TEs) to demonstrate the incoherent (i.e., intensity summation) and coherent (interference) contributions. Here, we show that these contributions obey rigorous sum rules. These relationships not only provide physical insights into DEs, but also may play an important role in utilizing such channels for the most efficient energy delivery in experiments.

Deposition matrix. We consider a continuous wave of single frequency at which the material dispersion and absorption of light are negligible. Figure 1 illustrates two geometries for energy delivery into a linear scattering system: (a),(b) wide slab with open (leaky) boundary, (c),(d) narrow waveguide with closed (reflecting) sidewalls. The deposition matrix (DM) $\mathcal{Z}$ is introduced for a target region of arbitrary size, shape, and depth [11]. It relates an orthonormal set of input waves to the corresponding spatial field distributions within the target region. As illustrated in Fig. 1(a) of a wide slab, the orthogonal input modes have distinct wave vectors, while in Fig. 1(c), the input waves are a complete set of waveguide modes. The total number of input modes is N. With a unit flux of incident light in the nth mode, the complex field distribution throughout the scattering system is $E_n^{(0)}(\vec{r})$. We sample the fields uniformly across a target region of volume $\mathcal{V}$ centered at $\vec{r}_D$, see Fig. 1(a). The field at the mth sampling point $\vec{r}_m$ is $E_n^{(0)}(\vec{r}_m;\vec{r}_D)$, where $m = \{1,\ldots,M\}$. The volume $\mathcal{V}/M$ covered by each sampling point is much smaller than λ^3, where λ is the wavelength. The deposition matrix of dimension $M \times N$ is defined as

$$\mathcal{Z}_{mn}(\vec{r}_D) \equiv \left[\epsilon(\vec{r}_m)\,\frac{\mathcal{V}}{M}\right]^{1/2} E_n^{(0)}(\vec{r}_m;\vec{r}_D)\,, \tag{1}$$

where $\epsilon(\vec{r})$ is the spatially varying dielectric constant.

The deposition eigenchannels are obtained from the singular value decomposition (SVD), $\mathcal{Z}_{mn}(\vec{r}_D) = \sum_{\alpha=1}^{N} U_{m\alpha}^{(D)}(\vec{r}_D)\,\zeta_\alpha^{1/2}(\vec{r}_D)\left[V_{n\alpha}^{(D)}(\vec{r}_D)\right]^*$. Here, $\zeta_\alpha(\vec{r}_D)$ and $V_{n\alpha}^{(D)}(\vec{r}_D)$ are the eigenvalue and eigenvector of matrix $\mathcal{Z}^\dagger(\vec{r}_D)\mathcal{Z}(\vec{r}_D)$, respectively. The incident wavefront $V_{n\alpha}^{(D)}(\vec{r}_D)$ excites the αth eigenchannel $E_\alpha^{(D)}(\vec{r};\vec{r}_D) = \sum_{n=1}^{N} E_n^{(0)}(\vec{r})\,V_{n\alpha}^{(D)}(\vec{r}_D)$ inside the system. Using the unitarity of matrices $U^{(D)}(\vec{r}_D)$ and $V^{(D)}(\vec{r}_D)$ as well as the definition of $\mathcal{Z}(\vec{r}_D)$ in Eq. (1), we get an explicit relationship for the eigenvalue (see

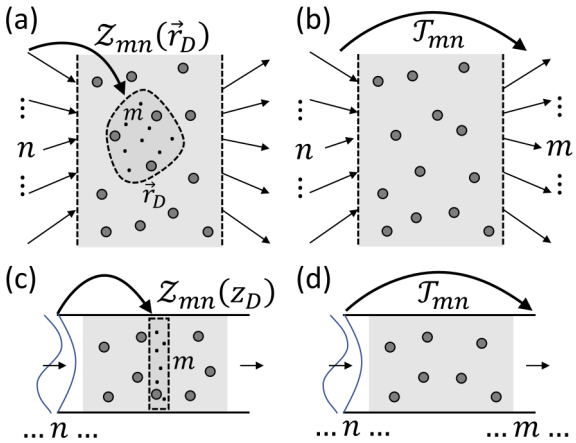

Fig. 1. Schematic depiction of (a),(b) the slab and (c),(d) the waveguide scattering-medium geometries. The deposition matrix relates the input to the internal fields inside a scattering medium, panels (a),(c). The transmission matrix $\mathcal{T}_{mn}$ relates the input and output degrees of freedom, panels (b),(d).

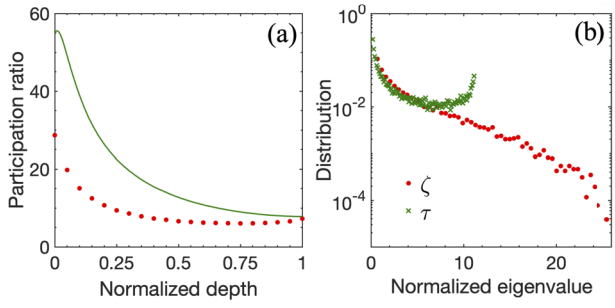

Fig. 2. Numerical simulations in a 2D disordered waveguide (Supplement 1). (a) Intensity participation ratio $\mathcal{P}^{(D)}(z = z_D; z_D)$ for DEs (circles) is consistently below $\mathcal{P}^{(T)}(z = z_D)$ for the TEs (solid line) at different depths. (b) Probability density of the deposition (red circle) and transmission (green cross) eigenvalues for a slice target at the depth $z_D = L/2$ (Supplement 1). Compared to TEs, fewer DEs have larger eigenvalues and bigger contributions to local intensities, leading to their lower participation ratios in panel (a).

Supplement 1):

$$\zeta_\alpha(\vec{r}_D) = \frac{\mathcal{V}}{M}\sum_{m=1}^{M}\epsilon(\vec{r}_m)\left|E_\alpha^{(D)}(\vec{r}_m;\vec{r}_D)\right|^2. \tag{2}$$

This relationship reveals that the deposition eigenvalue is equal to the total energy inside the target region with a coherent excitation of $E_\alpha^{(D)}(\vec{r};\vec{r}_D)$.

For comparison, Figs. 1(b) and 1(d) show the transmission matrix $\mathcal{T}$ that maps the incident fields to the transmitted fields. When a monochromatic light with a unit flux in the nth mode is incident to the scattering system, $|\mathcal{T}_{mn}|^2$ is the amount of flux carried away by the mth outgoing mode in transmission. TEs are obtained from the SVD $\mathcal{T}_{mn} = \sum_{\alpha=1}^{N} U_{m\alpha}^{(T)} \cdot \tau_\alpha^{1/2} \cdot \left[V_{n\alpha}^{(T)}\right]^*$. The input and output wavefronts of the αth TE are given by $V_{n\alpha}^{(T)}$ and $U_{m\alpha}^{(T)}$, and the transmittance by eigenvalue τ_α. Similar to the DEs above, the incident wavefront $V_{n\alpha}^{(T)}$ excites the αth TE $E_\alpha^{(T)}(\vec{r}) = \sum_{n=1}^{N} E_n^{(0)}(\vec{r})\, V_{n\alpha}^{(T)}$ inside the system.

Sum rules for deposited energy. Singular value decomposition is a linear transformation of the input basis that yields an orthonormal set defined by the unitary matrix $V^{(D)}(\vec{r}_D)$ or $V^{(T)}$ for the deposition and transmission, respectively. This orthonormal property of the input eigenvectors $V_{n\alpha}^{(D)}(\vec{r}_D)$ and $V_{n\alpha}^{(T)}$ has a profound impact on the distribution of the wave intensity *inside* the scattering medium. Summing the intensity of all eigenchannels at any given point $\vec{r}$ gives (see Supplement 1)

$$\sum_{\alpha=1}^{N}\left|E_\alpha^{(D)}(\vec{r};\vec{r}_D)\right|^2 = \sum_{\alpha=1}^{N}\left|E_\alpha^{(T)}(\vec{r})\right|^2 = \sum_{n=1}^{N}\left|E_n^{(0)}(\vec{r})\right|^2. \tag{3}$$

This means the sum of intensities excited by any complete set of input wavefronts, such as those of DEs or TEs, remains the same. The above relationships lead to two remarkable properties. First, the physical quantity being preserved by an SVD transformation is the sum of field intensity. Because Eq. (3) holds at every position, and thus can be multiplied by $\epsilon(\vec{r})$ from both sides, it can be interpreted as *point-wise* (i.e., local) conservation of energy. Second, the above relationship is not statistical—it does not involve any statistical averaging over an ensemble of disorder realizations, instead, it holds for every realization.

Equation (3) has another important implication—a large enhancement of energy deposition means only a small number of eigenchannels make dominant contributions to the sum and the rest of the contributions are negligible. This can be quantified by the intensity participation ratio $\mathcal{P}^{(D)}(z, z_D) = \left(\sum_{\alpha=1}^{N}\left|E_\alpha^{(D)}(z; z_D)\right|^2\right)^2 / \left(\sum_{\alpha=1}^{N}\left|E_\alpha^{(D)}(z; z_D)\right|^4\right)$ for DEs, and $\mathcal{P}^{(T)}(z) = \left(\sum_{\alpha=1}^{N}\left|E_\alpha^{(T)}(z)\right|^2\right)^2 / \left(\sum_{\alpha=1}^{N}\left|E_\alpha^{(T)}(z)\right|^4\right)$ for TEs [12]. Here, $\mathcal{P} = N$ when all contributions are equal and $\mathcal{P} = 1$ when only one out of N channels contribute. Figure 2(a) plots $\mathcal{P}^{(D)}(z = z_D; z_D)$ and $\mathcal{P}^{(T)}(z = z_D)$ versus z_D obtained numerically (see Supplement 1) for a 2D disordered waveguide system in Figs. 1(c) and 1(d). A lower participation ratio for DEs, in combination with the sum rule in Eq. (3), leads to a higher enhancement of the cross section integrated intensity at the target depth $z = z_D$, as observed in Ref. [11]. Alternatively, the extraordinarily large intensities of a few DEs, in turn, allow for the minimal intensity to be even below that of the lowest-transmission eigenchannel at the same depth. Furthermore, because Eq. (2) relates the local intensity of DEs to their eigenvalues, their probability density function (PDF) exhibits a heavy tail toward the large value of $\zeta_{max}(\vec{r}_D)/\langle\zeta(\vec{r}_D)\rangle$, see Fig. 2(b). In contrast, the PDF of the transmission eigenvalues $P(\tau)$ has the celebrated bimodal distribution [13]. It has one peak at $\tau_\alpha \sim 0$ and a smaller peak at $\tau_\alpha \sim 1$. Transmission eigenvalues have an upper bound of 1 due to flux conservation, whereas deposition eigenvalues have no such constraint. The eigenvalue repulsion leads to the peak of $P(\tau)$ at 1 and a long tail of $P(\zeta)$ at large ζ, c.f., Fig. 2(b). Importantly, the enhancement of DEs $\zeta/\langle\zeta\rangle$ exceeds that of TEs $\tau/\langle\tau\rangle$, as observed in Ref. [11]. This is consistent with a smaller participation ratio of DEs in Fig. 2(a) and their higher local intensity enhancement than TEs, see Fig. 3. All of these conclusions are indeed supported by the results in Ref. [11], demonstrating that a combination of the knowledge of the eigenvalue PDF and the constraints imposed by Eq. (3) has important implications for local energy density enhancement inside a random scattering system.

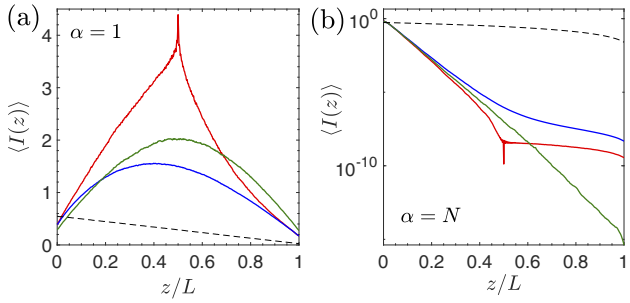

Fig. 3. Cross-section-averaged intensity profile of DE (red) in disordered waveguide geometry (see Supplement 1) for $z_D = L/2$ and its incoherent component (blue) is compared to the corresponding TE (green). Panels (a) and (b) correspond to the highest (eigenchannel $\alpha = 1$) and lowest (eigenchannel $\alpha = N$) eigenvalue, respectively. A random input intensity profile (dashed line) is shown for reference. Around the target region, the enhancement/suppression of the local intensity of DE above/below that of the maximum/minimum TE is observed. The incoherent part, however, is below/above the maximum/minimum TE.

We also find the sum rule for the deposition eigenvalues. Summing over $\zeta_\alpha(\vec{r}_D)$ and recalling Eq. (3), we obtain

$$\begin{aligned}\sum_{\alpha=1}^{N}\zeta_\alpha(\vec{r}_D) &= \frac{\mathcal{V}}{M}\sum_{m=1}^{M}\epsilon(\vec{r}_m)\left[\sum_{\alpha=1}^{N}\left|E_\alpha^{(D)}(\vec{r}_m;\vec{r}_D)\right|^2\right]\\ &= \frac{\mathcal{V}}{M}\sum_{m=1}^{M}\epsilon(\vec{r}_m)\left[\sum_{\alpha=1}^{N}\left|E_\alpha^{(T)}(\vec{r}_m)\right|^2\right]\\ &= \frac{\mathcal{V}}{M}\sum_{m=1}^{M}\epsilon(\vec{r}_m)\left[\sum_{n=1}^{N}\left|E_n^{(0)}(\vec{r}_m)\right|^2\right].\end{aligned} \tag{4}$$

This equation shows that the sum of all deposition eigenvalues is equal to a sum of local energies (sampled over M points $\{\vec{r}_m\}$) for all DEs, TEs or, more generally, excited by any orthogonal set of input wavefronts.

Therefore, the sum of all deposition eigenvalues gives the total energy within the target region excited by all input degrees of freedom. Moreover, the degree of control of the energy delivery via DEs is determined by the PDF of deposition eigenvalue $P(\zeta)$. In diffusive systems, $P(\zeta)$ is amenable to a theoretical description within the framework of filtered random matrix (FRM) theory [11,14], which thus provides information about the maximal and minimal energies achievable at the target.

Interference of transmission eigenchannels. The intensity sum rule in Eq. (3) does not imply that one set of eigenchannel intensity profiles, e.g., DEs', is a linear superposition of the *intensity* profiles for another set, e.g. of TEs'. For example, a linear combination of $\left|E_n^{(0)}(\vec{r})\right|^2$, which all decay with depth, cannot be superimposed to represent the maximum TE profile $\left|E_\alpha^{(T)}(\vec{r})\right|^2$, which is peaked in the middle of the system. In Ref. [11], we demonstrated that the interference between channels inside the scattering system is responsible for the diverse intensity profiles of different eigenchannels. Here, we are specifically interested in a relationship between DEs and TEs. The *field* patterns of the two eigenchannels are related via a linear transformation:

$$E_\alpha^{(D)}(\vec{r};\vec{r}_D) = \sum_{\beta=1}^{N} E_\beta^{(T)}(\vec{r}) d_{\beta\alpha}(\vec{r}_D), \tag{5}$$

where the decomposition coefficient $d_{\beta\alpha}(\vec{r}_D) = \sum_{n'=1}^{N}[V_{\beta n'}^{(T)}]^* V_{n'\alpha}^{(D)}(\vec{r}_D)$ represents a projection of the input vector of the αth DE onto that of the βth TE. Using these decomposition coefficients, the intensity pattern of a DE can be expressed as two distinct terms:

$$\left|E_\alpha^{(D)}(\vec{r};\vec{r}_D)\right|^2 = \sum_{\beta=1}^{N}\left|E_\beta^{(T)}(\vec{r})\right|^2 |d_{\beta\alpha}|^2 \tag{6}$$

$$+\sum_{\beta\neq\beta'}^{N} d_{\beta\alpha}\, d_{\alpha\beta'}^{*} E_\beta^{(T)}(\vec{r})\left[E_{\beta'}^{(T)}(\vec{r})\right]^*. \tag{7}$$

The first term is an incoherent sum of TE intensity patterns, whereas the second term is the result of interference between different TEs inside the scattering medium. The numerical simulation results in Figs. 3(a) and 3(b) illustrate that the interference contributions can be positive or negative to enhance or suppress the energy in the target. These contributions provide a physical mechanism to enhance the local energy above that of the largest-transmission eigenchannel or below that of the smallest-transmission eigenchannel.

The quantity $|d_{\beta\alpha}|^2$ represents the incoherent (i.e., a real positive intensity) contribution due to βth TE to the αth DE. We obtain the sum rule (see Supplement 1):

$$\sum_{\beta=1}^{N}|d_{\beta\alpha}|^2 = 1 = \sum_{\alpha=1}^{N}|d_{\beta\alpha}|^2. \tag{8}$$

This is a non-trivial result, since $|d_{\beta\alpha}|^2$ cannot be interpreted as a weight coefficient due to presence of the interference term in Eq. (7). Furthermore, it leads to an important constraint on this very term. By summing both sides of that equation and using Eqs. (3) and (8), we get

$$\sum_{\alpha=1}^{N}\left[\sum_{\beta\neq\beta'} d_{\beta\alpha}\, d_{\alpha\beta'}^{*} E_\beta^{(T)}(\vec{r})\left[E_{\beta'}^{(T)}(\vec{r})\right]^*\right] \equiv 0. \tag{9}$$

As shown in Ref. [11], the interference contribution can be quite large, even dominant in some cases. The relationship in Eq. (9) states that the sum of interference contributions to all DEs is, in fact, zero. To illustrate this point, we plot (see Supplement 1) in Fig. 4 the coherent contributions at the target depth $z_D = L/2$ for all DEs. Each contribution is normalized by $(1/N)\sum_{n=1}^{N}\left\langle\left|E_n^{(0)}(z_D)\right|^2\right\rangle$, which represents the unoptimized intensity at the target depth. A small number of DEs have large positive contributions. In contrast, the number of small negative contributions is large to ensure the sum is equal to 0 in Eq. (9).

Again, we stress that the above relationships apply to every disorder configuration and do not require any statistical averaging. Furthermore, because the left-hand side of Eq. (7) is a positively defined quantity, we note that

$$\sum_{\beta=1}^{N}\left|E_\beta^{(T)}(\vec{r})\right|^2 |d_{\beta\alpha}|^2 \geq -\sum_{\beta\neq\beta'}^{N} d_{\beta\alpha}\, d_{\alpha\beta'}^{*} E_\beta^{(T)}(\vec{r})\left[E_{\beta'}^{(T)}(\vec{r})\right]^*. \tag{10}$$

It illustrates that when the interference contribution does become negative, i.e., for a low-deposition eigenchannel, it cannot exceed in absolute value the incoherent contribution, i.e., it cannot become dominant, see the inset in Fig. 4. However, such restriction does not apply for the high-deposition eigenchannel with positive coherent contribution, which can and, in fact, does become dominant in a diffusive medium for the deposition depth

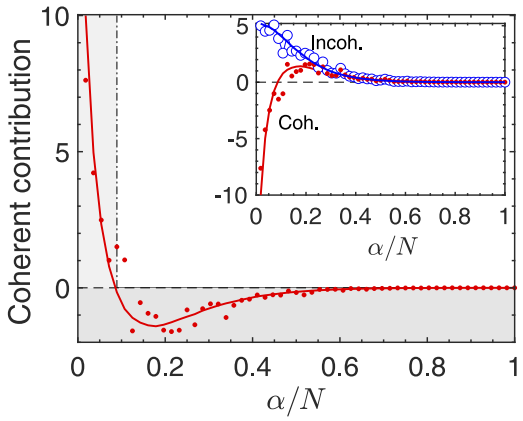

Fig. 4. Coherent contribution in Eq. (7) for each DE α, computed at $z = z_D$ in the numerical model (see Supplement 1), is shown in the main plot. A small number of large positive contributions is balanced by a large number of smaller negative contributions in accordance with Eq. (9). The inset shows that, when negative, the coherent contribution (red) cannot exceed the incoherent one (blue) in absolute value, see Eq. (10). In both plots, symbols/lines represent one disorder realization/statistically averaged results, respectively.

$z_D < L/2$, c.f., Fig. 4 and Ref. [11]. We note that such larger positive interference contributions are related to the PDF of the deposition eigenvalues. Since the PDF $P(\zeta)$ has a long tail at large ζ in diffusive systems, the number of positive contributions is small. Consequently, the sum rule in Eq. (9) dictates that such contributions must be large to balance the numerous negative ones.

Conclusions. Targeted delivery of electromagnetic energy inside a random-scattering system has important applications in imaging, optogenetics, photothermal therapy, etc. DEs accomplish the goal of delivering maximal or minimal amount of energy to a target region of arbitrary size, shape, and depth. Little is known about the spatial structure of the deposition eigenchannels, albeit some progress has been made in understanding the spatial distribution of TEs [12,15–18]. The PDF of deposition eigenvalues has been predicted by the filtered random matrix theory [11]. The sum rules, presented in this work, establish a connection between the spatial structure of DEs and the eigenvalues. They represent the rigorous constraints for any disorder realization of 2D and 3D scattering systems in both waveguide and slab geometry. We note that material dispersion is neglected in this study of monochromatic light. It would be interesting to extend the sum rules for dispersive materials and broadband light, and also explore the limitation due to incomplete channel control of excitation.

Funding. National Science Foundation, Directorate for Mathematical and Physical Sciences (DMR-1905442, DMR-1905465).

Disclosures. The authors declare no conflicts of interest.

Data availability. All data underlying the results is presented in this paper.

Supplemental document. See Supplement 1 for supporting content.

REFERENCES

1. P. A. Mosk, A. Lagendijk, G. Lerosey, and M. Fink, Nat. Photonics **6**, 283 (2012).
2. H. Yu, J. Park, K. Lee, J. Yoon, K. Kim, S. Lee, and Y. K. Park, Curr. Appl. Phys. **15**, 632 (2015).
3. J. Kubby, S. Gigan, and M. Cui, *Wavefront Shaping for Biomedical Imaging* (Cambridge University Press, 2019).
4. S. Gigan, O. Katz, and H. B. de Aguiar, *et al.*, J. Phys. Photonics **4**, 042501 (2022).
5. S. Rotter and S. Gigan, Rev. Mod. Phys. **89**, 015005 (2017).
6. I. M. Vellekoop, Opt. Express **23**, 12189 (2015).
7. S. M. Popoff, G. Lerosey, R. Carminati, M. Fink, A. C. Boccara, and S. Gigan, Phys. Rev. Lett. **104**, 100601 (2010).
8. R. Horstmeyer, H. Ruan, and C. Yang, Nat. Photonics **9**, 563 (2015).
9. S. Yoon, M. Kim, M. Jang, Y. Choi, W. Choi, S. Kang, and W. Choi, Nat. Rev. Phys. **2**, 141 (2020).
10. X. Cheng and A. Z. Genack, Opt. Lett. **39**, 6324 (2014).
11. N. Bender, A. Yamilov, A. Goetschy, H. Yilmaz, C. W. Hsu, and H. Cao, Nat. Phys. **18**, 309 (2022).
12. M. Davy, Z. Shi, J. Park, C. Tian, and A. Z. Genack, Nat. Commun. **6**, 6893 (2015).
13. O. N. Dorokhov, Solid State Commun. **51**, 381 (1984).
14. A. Goetschy and A. D. Stone, Phys. Rev. Lett. **111**, 063901 (2013).
15. O. S. Ojambati, H. Yilmaz, A. Lagendijk, A. P. Mosk, and W. L. Vos, New J. Phys. **18**, 043032 (2016).
16. M. Koirala, R. Sarma, H. Cao, and A. Yamilov, Phys. Rev. B **96**, 054209 (2017).
17. R. Sarma, A. Yamilov, S. Petrenko, Y. Bromberg, and H. Cao, Phys. Rev. Lett. **117**, 086803 (2016).
18. N. Bender, A. Yamilov, H. Yilmaz, and H. Cao, Phys. Rev. Lett. **125**, 165901 (2020).